VISION-BASED TECHNIQUES FOR REFRACTION ANALYSIS IN APPLICATIONS OF TERRESTRIAL GEODESY

Philipp FLACH
Dipl.-Eng., Institute of Geodesy and Photogrammetry
Geodetic Metrology and Engineering Geodesy
Swiss Federal Institute of Technology
ETH Hoenggerberg
CH-8093 Zurich
E-mail: flach@geod.ethz.ch
SWITZERLAND

Hans-Gerd MAAS
Dr., Faculty of Civil Engineering and Geo Sciences
Section of Photogrammetry and Remote Sensing
Delft University of Technology
Thijsseweg 11
2629JA Delft
E-mail: h.-g.maas@geo.tudelft.nl
THE NETHERLANDS

KEY WORDS: Image sequences, least squares matching, refraction, air scintillation, digital levelling

ABSTRACT: Imaging sensors are increasingly spread in geodetic instruments, because they enable the evaluation of digital image data for the determination of direction and height. Beyond this, the analysis of temporal changes of image data may provide additional information about the refractivity in the atmosphere. Today, the refraction is still the decisive precision limiting factor in geodesy. This paper presents a method for the simultaneous measurement of refraction influences by the analysis of image sequences of a video-theodolite. This analysis is based on the model of optical turbulence which connects the meteorological parameter C_n^2 and l_0 (which are required for refraction detection) with fluctuations of the incoming waves, where these fluctuations can be measured by use of image processing techniques like least squares matching. A field experiment using a video-theodolite, a scintillometer, and a digital level is presented to show the potential of this method.

ZUSAMMENFASSUNG: In Instrumenten der terrestrischen Geodäsie sind bildbasierende Techniken zunehmend verbreitet, da sie die Auswertung von Bilddaten für die Richtungs- und Höhenbestimmung ermöglichen. Darüber hinaus kann die Analyse der zeitlichen Änderungen von Bilddaten zusätzliche Informationen über die Refraktionsverhältnisse in der Atmosphäre liefern. Heutzutage ist die Refraktion immer noch der entscheidende limitierende Faktor für die Genauigkeit in der Geodäsie. Daher wird in diesem Beitrag eine Methode für das simultane Messen von Refraktionseinflüssen mittels der Analyse von Bildsequenzen vorgestellt. Diese Methode basiert auf dem Modell der optischen Turbulenz, das die meteorologischen Parameter C_n^2 und l_0 (welche für die Bestimmung der Refraktion nötig sind) mit Fluktuationen der eintreffenden Wellen verknüpft, wobei diese Fluktuationen mittels Bildverarbeitung wie least squares matching gemessen werden können. Ein Feldexperiment mit einem Videotheodoliten, einem Szintillometer und einem Digitalnivellier wird präsentiert, um das Potential dieser Methode aufzuzeigen.

1. INTRODUCTION

Due to automation of tasks in terrestrial geodesy, image sensors and vision-based techniques have been increasingly spread into numerous geodetic instruments. For instance, CCD-sensors are built into tracking tacheometers and digital levels. Although image sensors and progressing instrument technology in general allow a high degree of precision and automation, the precision in the field of terrestrial measurement methods is still limited on account of atmospheric influences. The refractive influences of the atmosphere are especially crucial in consideration of direction transfer and levelling. So this contribution will focus on these fields of application in terrestrial geodesy.

1.1 Visualization of refraction influences

If optical geodetic measurements are performed in boundary air layers, the propagation of the sight beam is affected by refraction index gradients which are mainly the result of temperature gradients.
These gradients simultaneously occur with the turbulent motion of air parcels. The parcels' motion causes the scintillation (i.e., rapid changes of intensity of incoming light rays) of the target image in the telescope of geodetic instruments. The scintillation of the target image can basically be visualized as an image blurring and as displacements of image structures in image sequences. Within the scope of our research work, vision-based techniques are applied to determine appropriated parameters quantifying turbulent motions to model refraction influences and to reduce them simultaneously with the geodetic observation.

1.2 Previous work

In the field of geometric levelling, the visualization of refraction influences can be realized as the movements of scale lines of the leveling rods as seen through the level telescope. A practical experiment during 48 hours showed quite a good correlation between these movements and the temperature gradient (Kukkamäki, 1950). The fundamental theories of optical propagation in a turbulent medium were mainly developed in Russia (Tatarskii, 1971) and, for this reason, reports of the practical experiments for geodetic applications came from there as well (Vinogradov *et al.*, 1985). Despite the simple visual methods, they achieved a reduction of the systematic distortions up to about 80%. In doing this, the theoretical formulations were not applied entirely rigorously but were partially replaced by semi-empirical modelling. Additionally, it was shown that the vertical temperature profile along the line of sight can be combined with the movements of the target as seen through the telescope (Brunner, 1980). This mostly theoretical research work showed that refraction detection is possible in principle.
For the last twenty years, the potential of electronic data processing has been developed to the point that further applications in regard to the derivation of turbulence parameters from geodetic observations could also be carried

out. In doing so, several experimental setups have been developed using either a position-sensitive semiconductor diode (Huiser, Gächter, 1989) or a modified distance meter (Hennes, 1995) or a CCD camera (Casott *et al.*, 1998).

2. MODELLING OF REFRACTION INFLUENCES

2.1 Temperature gradients and optical turbulence

The refractive influences are primarily caused by local gradients in the temperature field of the atmosphere which change the propagation of light. The modeling of these effects is rather sophisticated since the temperature field is to be parameterized in a function of the light propagation path. In the following, we assume that direct measurements of the temperature gradient field are not available because the required precision of temperature measurements lies in the range of some 1/100 °C and, thus, measurements with use of temperature sensors are fairly demanding.
An alternative method to determine the vertical temperature gradient is the analysis of optical turbulence which can be detected as the scintillation of a laser beam or scintillation of image structures of targets. The correlation between temperature gradients and optical turbulence can be outlined as follows (Flach, Hennes, 1998a): The subsoil is warmed through IR radiation (sun) so that the lower strata of air have higher temperatures and, therefore, rise. The amount of rising air parcels (eddies) increases with increasing temperature gradient according to the buoyancy principle (cf. section 2.3). During this process, the air parcels behave like eddies producing smaller ones due to friction effects. This eddy formation is usually described with the three-dimensional spectrum of refractive index (Figure 1). As a consequence of the energy distribution of the spectrum of refractive index, the size of the eddies in the boundary air layers varies and this variation influences the propagation of an electro-optic wave. This phenomena can be observed as optical turbulence as follows: At the receiver point, changes in intensity are perceived as scintillation and, additionally, disturbances of the phase front of the wave front are recognized as changes in position of the target. Both effects can be measured by vision-based technologies with use of image sensors which can be built into geodetic instruments.

2.2 Structure constant C_n^2 and wave equation

The changes in refractive index caused by temperature fluctuations are usually smooth random functions of both time and space. Thus, the distribution of the refractive index $n(\mathbf{r}, t)$ can only be determined by certain averages or mean quantities, such as the structure constant C_n^2 of the refractive index fluctuations which is defined as

$$C_n^2(\mathbf{r}) = \frac{\langle n(\mathbf{r}_1) - n(\mathbf{r}_2) \rangle^2}{|\mathbf{r}|^{2/3}} \qquad [\mathrm{m}^{-2/3}] \tag{1}$$

where $\mathbf{r} = \mathbf{r}_1 - \mathbf{r}_2$ and the angle brackets indicate an ensemble average of the refractive index difference at the places $\mathbf{r}_1$ and $\mathbf{r}_2$, respectively. In the following, we assume that the random process generating the changes in refractive index is isotropic, then $C_n^2(\mathbf{r}) = C_n^2(|\mathbf{r}|) = C_n^2(r)$.

Because polarization fluctuations can be neglected, the propagation of the electric field $E(\mathbf{r}, t)$ in atmospheric turbulence is described by the scalar wave equation (HELMHOLTZ equation):

$$\nabla^2 E + k^2 n^2 E = 0 \tag{2}$$

To solve this equation, the refractive index $n(\mathbf{r}, t)$ which is a random variable must be described by use of the power spectrum density of n (turbulence spectrum).

2.3 Turbulence spectrum

The refractive index spectrum Φ_n quantifies the optical turbulence in the boundary layer of the atmosphere. The spectrum is modeled by the inner scale l_0 (= smallest diameter of the occurring eddies), the outer scale L_0 (= largest diameter of the occurring eddies) and the structure constant C_n^2 of refractive index fluctuations, where the function of the refractive index spectrum the is given by the following formulae (Tatarskii, 1971):

$$\Phi_n(k) = 0.033 C_n^2 k^{-11/3} e^{-(l_0 \cdot k)^2 / 5.92^2} \tag{3}$$

or more elaborated (Hill, Clifford, 1978):

$$\Phi_n(k) = 0.033 C_n^2 \left(k^2 + L_0^{-2}\right)^{-11/6} f_\Phi(k, l_0) \tag{4}$$

with

k	wave number		$[\mathrm{m}^{-1}]$
k	$= 2\pi/l$		(5)
l	diameter of eddies		[m]
f_Φ	decay of refractive index fluctuations in dissipation range		[-]
L_0	$\cong h/2$	(Hufnagel, 1978)	[m] (6)
h	distance from the ground		[m]

The graphs of these refractive index spectra are plotted in Figure 1. The graph shows that the so-called inertial range includes eddies with a diameter between l_0 ($\cong$ 3 mm) and L_0 ($\cong$ 1 m).
In the inertial range, the kinetic energy associated with the larger eddies is redistributed without loss of energy to successively smaller and smaller eddies until finally the diameter is smaller than l_0 and the eddies are dissipated by viscosity. Over the inertial range, the spectrum shows a slope of –11/3 and an offset of C_n^2 (logarithmic plot).
If the parameters C_n^2 and l_0 of the spectrum of refractive index are measured and the level of the line of sight above ground is approximately known, the amount of the turbulent energy fluxes can be determined using the Monin-Obukov-similarity relation (Hill, 1996).
Since the turbulent energy fluxes are related with the temperature gradient field, the temperature gradient can be computed integrally along the line of sight and the refraction influences can be corrected (Deussen, 1998). Hereby, it is assumed that the temperature gradient field is statistically homogeneous along the line of sight.

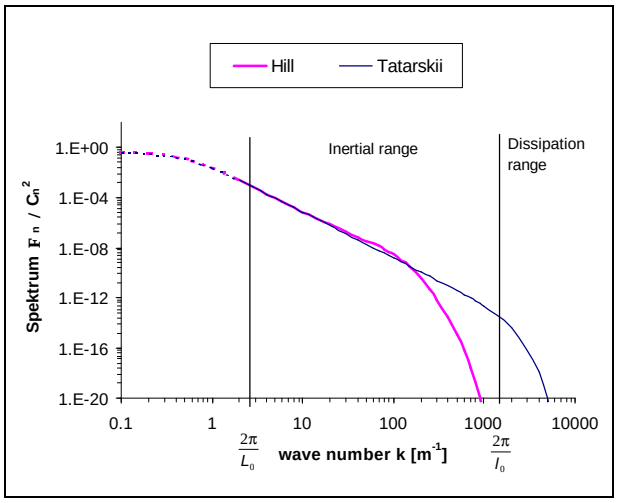

Figure 1: Two models of spectrum of refractive index (Dotted line: Not yet confirmed by experiments)

3. MEASUREMENT METHODS

3.1 Reference measurements

Reference measurements are required for the experiment described below (section 4) to compare the results with measurements performed with image sensors (video-theodolite). The scintillometer is a field-tested instrument to obtain reference measurements for the parameters C_n^2 and l_0 of optical turbulence. The instrumental setup of the scintillometer is shown in Figure 2.

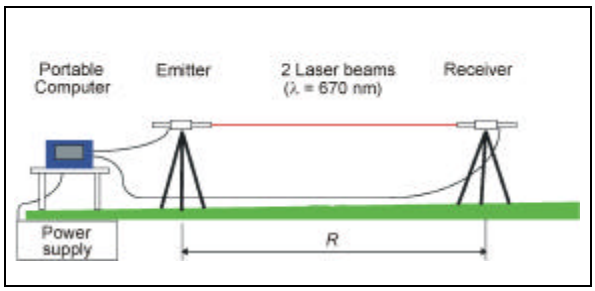

Figure 2: Scintillometer to measure optical turbulence (distance R = 86m)

The emitter of the scintillometer emits two parallel beams to the receiver. Random fluctuations of refractivity in the atmosphere cause the intensity of the received light power of the two beams to fluctuate randomly over time. The variances and covariances of the respective intensities are evaluated to derive both, the structure constant C_n^2 and the inner scale l_0 (Thiermann, 1992).

3.2 Image sensor

As a geodetic field instrument, the video-theodolite Leica TM3000V enables the acquisition of image series which are the starting point for determining the structure constant C_n^2 and the inner scale l_0. The video-theodolite has an integrated CCD-array sensor which is configured as shown in Figure 3.

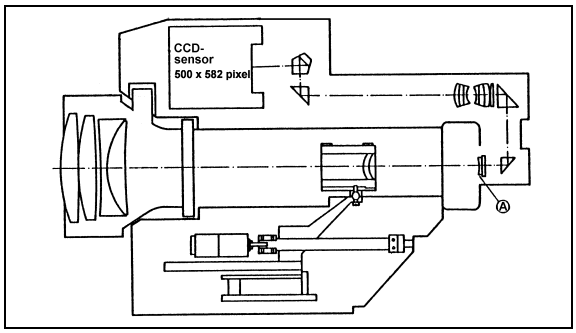

Figure 3: Video-theodolite with integrated CCD-sensor

The internal reference frame coincides with the plane of the reticle (A) and appears on each video image in order to give reference points for the local coordinate system of the image. A series of 25 images of a static target pattern (e.g. levelling rod) are grabbed within one second and stored by an external field computer. The read-out frequency of 25 Hz suffices if the velocity of crosswind is lower than 0.1 m/s and the diameters of most of the eddies are larger than 8 mm (cf. Figure 1: spectrum of refractive index by Hill). These conditions are normally fulfilled on days with high temperature gradients, i.e., with high refraction influences.
For each series, the first image serves as a reference image and the positions of selected image regions of the reference image are determined in the subsequent images with use of least squares matching. The small changes of the position and further parameters determined by least squares matching are the base to calculate the structure constant C_n^2 and the inner scale l_0.

3.3 Least squares matching

Least squares matching (LSM) is an area-based matching technique, which is often used in photogrammetry for the establishment of correspondences between images from multiple viewpoints. LSM was first presented by (Förstner, 1984) and (Grün, 1985). It has also been used for the analysis of motion between subsequent frames of sequences of two-dimensional or three-dimensional images (Papantoniou/Dracos, 1989; Maas *et al.*, 1994).
LSM tries to determine the six coefficients of an affine transformation for a chosen patch in one image to its transformed counterpart in an other image by minimizing the sum of the squares of gray value differences. Formulated as a least-squares adjustment problem, the technique converges after a few iterations, provided sufficient contrast and good approximate values. The two shift parameters of the affine transformation represent a lateral movement of the patch; the four remaining parameters represent a deformation of the patch. Due to the redundancy in the estimation process, a covariance matrix containing information on standard deviations of the parameters and correlations between parameters is determined simultaneously; this allows for an analysis of the determinability and precision of the transformation parameters. Provided a good image quality, standard deviations of the shift parameters as small as 1/50 of the pixel size can be achieved by LSM.
In the application discussed here, the analysis can be reduced to a one-dimensional problem due to the characteristics of the phenomenon and the shape of the image

signal provided by a levelling rod. As a vertical scale parameter is very unlikely to be determinable over the small size of a patch, the analysis can be further reduced to the determination of one shift parameter a in vertical image direction. Hence, the model is given by:

$$g(x_i) = f(x_i - a) + e(x_i), \quad i = 1, ..., n \tag{7}$$

with
$f(x)$ function of the reference image signal
$g(x)$ function of the image signal at the corresponding position in the subsequent image
x_i position of the patch in the subsequent image
n number of pixels involved in the matching
$e(x)$ random noise with variance σ_0^2

Since the gray value functions f and g are not linear, an approximated value for the parameter a_0 is required:

$$a = a_0 + da \tag{8}$$

where da is the unknown correction to the approximated shift value. Thus, the function f is linearized around the point $(x_i - a_0)$ and yields to:

$$g(x_i) = f(x_i - a_0) - f_{x_i} da + e(x_i) \tag{9}$$

with

$$f_{x_i} = \frac{df(x)}{dx}\Big|_{x=x_i-a_0} \tag{10}$$

whereby the second order terms are assumed to be negligible. For the n pixels of the patches we then obtain the following linearized equations for each pixel:

$$\Delta g(x_i) = -f_{x_i} da + e(x_i), \quad i = 1, ..., n \tag{11}$$

with

$$\Delta g(x_i) = g(x_i) - f(x_i - a_0) \tag{12}$$

Using the least-squares method, the unknown correction da of the shift is given by

$$d\hat{a} = \frac{-\sum_{i=1}^{n} f_{x_i} \Delta g(x_i)}{\sum_{i=1}^{n} f_{x_i}^2} \tag{13}$$

and the estimated shift is

$$\hat{a} = a_0 + d\hat{a} \tag{14}$$

As an advantage of least squares matching in general, the full covariance matrix delivered by the matching procedure is available and allows for an analysis of the determinability and precision of the unknown parameters. In the one-dimensional situation, the precision of the total shift is calculated by

$$\sigma_{\hat{a}}^2 = \frac{\sigma_0^2}{\sum_{i=1}^{n} f_{x_i}^2} \tag{15}$$

If the one-dimensional model really holds and the number of observations n is large enough, the noise variance σ_0^2 can be estimated from the residuals of the least squares fit:

$$\hat{\sigma}_0^2 = \frac{1}{n-1} \sum_{i=1}^{n} \left[g(x_i) - f(x_i - \hat{a}) \right]^2 \tag{16}$$

The noise variance σ_0^2 can also be used as a measure for intensity fluctuations of the incoming light ray since strong changes of the intensity of the light ray increase the differences $g(x_i) - f(x_i - \hat{a})$ between the reference image and the subsequence image.

3.4 Determining turbulence structure parameters

3.4.1 Amplitude and phase fluctuations

To determine the turbulence structure parameters C_n^2 and l_0 with use of least squares matching, we first need the amplitude fluctuations and phase fluctuations of the incoming light beam. Hereby, we assume smooth perturbations of the incoming waves and neglect polarization effects, so the solution of (2) is given by

$$E = E_0 \cdot \exp\left[\chi(\mathbf{r},t) + \mathrm{i} \cdot S(\mathbf{r},t)\right] \tag{17}$$

where
E_0 unperturbed field of the wave
χ log-amplitude of the intensity I of the wave (natural logarithm)
S phase

The amplitude fluctuations and phase fluctuations are expressed by the variances σ_S^2 and σ_χ^2 and can be derived by the results of least squares matching as follows.
The variance σ_S^2 can be obtained from small displacements of the image structures (patterns), because the inhomogenities of the refractive index field $n(\mathbf{r}, t)$ produce distortions of the wave front. An aperture-confined part receives the distorted incoming wave front and measures the variance of the angle-of-arrival by means of an image sensor. Thus, the following equations are given by geometrical considerations:

$$\sigma_S^2 = K^2 a^2 \sigma_\alpha^2 \tag{18}$$

where

$$\sigma_\alpha^2 = \frac{p^2 \cdot \sigma_y^2}{f^2} \tag{19}$$

$$\sigma_y^2 = \frac{1}{r} \sum_{j=1}^{r} \hat{\sigma}_{y,j}^2 \tag{20}$$

and

$$\hat{\sigma}_{y,j}^2 = \frac{1}{m-1} \left[\sum_{i=1}^{m} y_{i,j}^2 - \frac{1}{m} \left(\sum_{i=1}^{m} y_{i,j} \right)^2 \right] \tag{21}$$

with
σ_α^2 variance of the angle-of-arrival of the incoming wave
K wave number ($K = 2\pi/\lambda$) [m^{-1}]

λ	wave length of incoming wave	[m]
a	aperture	[m]
p	pixel size of sensor	[m/pixel]
f	focal length	[m]
m	number of images (without reference image) of a series	
r	number of patches (selected image regions)	
$y_{i,j}$	position of the j-th patch in the i-th image [pixel]	

The variance σ_s^2 is mainly influenced by eddies, their diameter l being in the range of the aperture of the video-theodolite.
To determine the variance σ_χ^2, we may think of the eddies as random lenses. The lenses are randomly distributed in space and have a random size according the turbulent spectrum. Using geometrical optics, we can calculate the amplitude variations of the incoming waves due to these lenses. This leads to deviations in the intensity level of each pixel grabbed by the CCD-sensor which can be expressed by:

$$\sigma_\chi^2 = \frac{1}{4}\ln(\sigma_0^2 + 1)\cdot c_{Rad} \tag{22}$$

with

c_{Rad}	sensor specific constant for conversion of gray values into intensity of the beam.
σ_0^2	noise variance of least squares matching (a-posteriori estimation)

3.4.2 Determination of the structure constant C_n^2

The amplitude fluctuations σ_χ^2 and phase fluctuations σ_S^2 must be correlated with the turbulence spectrum in order to determine the turbulence structure parameters C_n^2 and l_0. For spherical waves in smoothly varying medium, the phase fluctuations σ_S^2 is given by (Lawrence, Strohbehn, 1970):

$$\sigma_s^2 = 8\pi^2 K^2 \int_0^{R}\int_0^{\infty} \kappa\cdot\Phi_n(\kappa)\left[1 - J_0\left(\frac{a\kappa r}{R}\right)\right]\cdot \cdot\cos^2\left[\frac{\kappa^2 r(R-r)}{2KR}\right]\mathrm{d}\kappa\,\mathrm{d}r \tag{23}$$

with

J_0	Bessel function of the first kind	
R	Propagation path length	[m]
r	spatial integration variable	[m]
κ	spectral integration variable	[m^{-1}]

Under the assumption $(\lambda R)^{1/2} << 2a << L_0$, it can be shown (Lawrence, Strohbehn, 1970) that equation ((23) can be simplified by:

$$\sigma_S^2 = 1.05\cdot C_n^2 a^{5/3} R K^2 \tag{24}$$

which is a good approximation for σ_S^2. Using (18) and (19), it follows:

$$\sigma_\alpha^2 = 1.05\cdot C_n^2 a^{-1/3} R \tag{25}$$

and

$$C_n^2 = \frac{p^2\cdot\sigma_y^2 a^{1/3}}{1.05 f^2 R} \quad [\mathrm{m}^{-2/3}] \tag{26}$$

3.4.3 Determination of the inner scale l_0

The determination of the inner scale l_0 presumes that the structure constant C_n^2 is calculated by (26) and the amplitude fluctuations σ_χ^2 are determined by (22). For spherical waves in smoothly varying medium, the amplitude fluctuations σ_χ^2 can be written as (Lawrence, Strohbehn, 1970):

$$\sigma_\chi^2 = 4\pi^2 K^2 \int_0^{R}\int_0^{\infty} \kappa\cdot\Phi_n(\kappa)\cdot\sin^2\left[\frac{\kappa^2 r(R-r)}{2KR}\right]\mathrm{d}\kappa\,\mathrm{d}r \tag{27}$$

The amplitude fluctuations σ_χ^2 depends on the inner scale l_0 because the refractive index spectrum Φ_n is a function of l_0. Unfortunately, an explicit equation between σ_χ^2 and l_0 is still not known. However, by numerically integrating of (27), a correlation between σ_χ^2/C_n^2 and $(\lambda R)^{1/2} / l_0$ can be revealed (Figure 4).

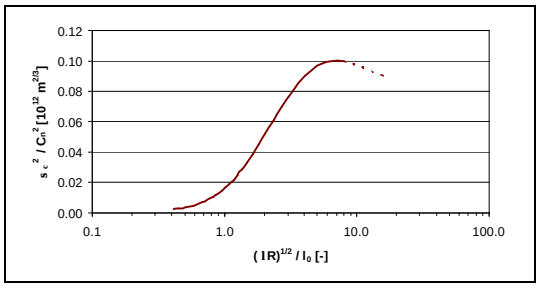

Figure 4: Correlation between σ_χ^2/C_n^2 and $(\lambda R)^{1/2}\, l_0^{-1}$ to determine l_0

Under the realistic assumption that the inner scale l_0 is not too small (i.e. $l_0 > 3$ mm), the results of the integration of (27) lead to the one to one correlation plotted in Figure 4 This correlation is not sensitive to the variation of the outer scale L_0 (Flach, Hennes, 1998b). Therefore, it can be stored in a look-up-table and is used to determine l_0.

4. EXPERIMENT

4.1 Instrumental setup

In regard to the experiment into the possible applicability in geodetic instruments, we compare the results of measurements which have been performed simultaneously by means of a video-theodolite (TM3000V, Leica Inc., Switzerland) and a scintillometer (SLS 20, Scintec Inc., Germany; Figure 2). The scintillometer which serves as the reference instrument was positioned parallel to the line of sight of the video-theodolite where the distance between the scintillometer and the video-theodolite was about 3 m.
In this field test, 102 image series of 25 images each (1 second per series) were produced over six hours with the help of the video-theodolite from a coded levelling rod positioned 86 meters away (Figure 5).
The first picture of each series was always defined as the reference image. The reference image allows to eliminate numerous influences such as the sun's altitude and optical distortions. For these reasons, it will suffice if the results

of the least squares matching are related to the reference image.

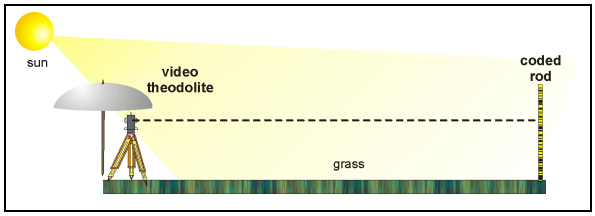

Figure 5: Field Measurements with video-theodolite

By using the least-squares algorithms described above, the positions of 37 chosen bar-code sections could be determined with subpixel-accuracy for each of the following 24 images.
Figure 6 shows a region of the coded levelling rod which is grabbed by use of the video-theodolite (f = 295 mm, pixel size (H x V) = 17 x 11 µm) over a distance of R = 86 m under turbulent atmospheric conditions.

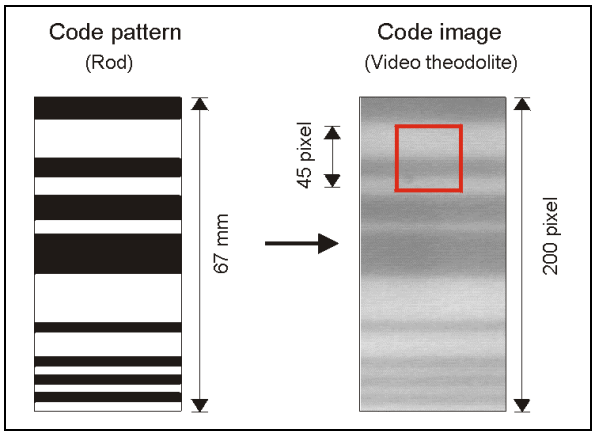

Figure 6: Code structure and code blurring

The square in the grabbed image of Figure 6 indicates a bar-code section (patch) which was used for the least squares matching evaluation.

4.2 Results

The least squares matching of the images grabbed by the video-theodolite provides on one hand the small displacements $y_{i,j}$ of the position of each patch in relation to the reference image of the correspondent series. Hereby, the standard deviation of the shift parameter σ_a is about 0.026 pixel (average), so that the detected displacements must be considered as significant. Using the equations (20), (21) and (26), the structure constant C_n^2 of the refractive index fluctuations is calculated and compared with the results of the scintillometer in Figure 7.
On the other hand, the least squares matching provides the variance σ_0^2 which is derived from the minimized sum of square differences by (16). Thus, the inner scale l_0 (diameter of the smallest eddy) can be calculated by (22) and the look-up-table displayed in Figure 4. Hence, the inner scale as a result of the measurements with the video-theodolite is compared with the results of the scintillometer in Figure 8.

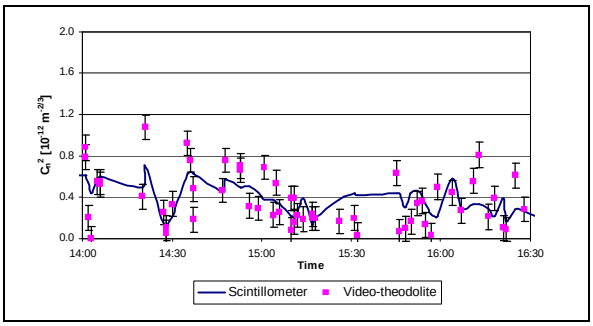

Figure 7: Comparison of structure constant C_n^2 with error bars (standard deviation)

The correlation coefficient between scintillometer and video-theodolite in the time series of C_n^2 amounts to r = 0.57 and in the time series of l_0 r = 0.45, respectively.

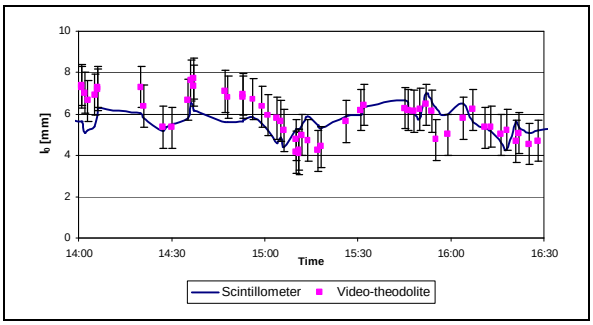

Figure 8: Comparison of inner scale l_0 with error bars (standard deviation)

It is seen that for atmospheric conditions the turbulence parameter C_n^2 and l_0 are subject to rapid temporal changes. Overall, the comparison indicates that the results provided by the video-theodolite and least-squares matching are in the same order of magnitude like the reference measurements of the scintillometer. However, discrepancies between the measurements of the scintillometer and of the video-theodolite can be observed. In the case of the inner scale l_0, deviations may be explained by averaging effects of the incoming wave since the aperture of the video-theodolite (a = 55 mm) is considerably larger than the aperture of the scintillometer (a = 2 mm). The discrepancies of the structure constant C_n^2 are to be considered in the perspective that the structure constant C_n^2 usually varies in the range of 10^{-16} to 10^{-12} $m^{-2/3}$, so the deviations seem acceptable.

4.3 Comparison with digital levelling

Since digital levels are widespread instruments in geodetic applications, we demonstrate the significance of influences of optical turbulence on digital levelling. Digital levels grab images of a coded rod by means of an integrated line scan sensor. The coded rod of the investigated digital level (SOKKIA SDL30) consists of a sequence of six different-width bars representing a 6-digit-code. The grabbed code pattern forms a unique code (5- or 8-bit code, depending on distance). In order to derive distance and height, the acquired series of figures are correlated with the code which is stored in the instrument. Hereby, the code image can be affected by optical turbulence as described above. In the field experiment mentioned

above, the digital level was positioned parallel to the emitter of the scintillometer and the coded rod next to the receiver of the scintillometer.
During the scintillometer measurements, at discrete points in time, the digital level performed seven subsequent height readings and the standard deviation of these readings were calculated and plotted in Figure 9.

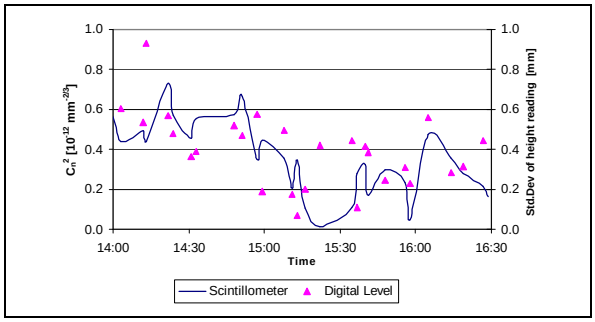

Figure 9: Comparison of scintillometer and digital level

We renounce to an exact mathematical model for the time being, and only point out that the time series of these two instruments are correlated (r = 0.54).
Although the correlation is not very high, the influence of optical turbulence in the applications of terrestrial geodesy is evident.

5. CONCLUSIONS

The presented experiment dealing with the images of a video-theodolite indicates that the method of least squares matching applied to image sequences provides similar results as scintillation measurements. Hence, vision-based technologies can also be utilized for refraction detection although there are still limitations in accuracy. A further advantage consists in the fact that image sensors have become rather familiar in geodetic instruments, so that the described methodology does not require exceptional instrumental expenditure.
Attention should be paid to the meteorological models which are used. For paths longer than 1000 meters (Lawrence, Strohbehn, 1970) the discussed algorithm is limited since the meteorological parameters are rarely statistically homogeneous and, therefore, it is difficult to derive the temperature gradient with the existing models. Thus, adapted meteorological models, which are currently being developed at the Swiss Federal Institute of Technology, are required to derive appropriated refraction corrections.

6. REFERENCES

Brunner, F. K., 1980. Systematic and Random Atmospheric Refraction Effects in Geodetic Levelling. In: Proc. of Second International Symposium on Problems Related to the Redefinition of North American Vertical Geodetic Networks., Ottawa (Canada), pp. 691-703.
Casott, N., Deussen, D., Witte, B., 1998. Methoden zur Bestimmung der geodätischen Refraktion bei terrestrischen Präzisionsmessungen. Vermessungswesen und Raumordnung, 60 (4), pp. 193-204.
Deussen, D., 1998. Modellansätze und Messmethoden zur Bestimmung des Brechungsindex-Gradienten der bodennahen Grenzschichtströmung. In: Freeden W. (ed.), Progress in Geodetic Science, Proceedings to Geodätische Woche Kaiserslautern (Germany), pp. 42-50.
Flach, Ph., Hennes, M., 1998a. Image processing techniques for determination of refraction influences. Symposium on Geodesy for Geotechnical and Structural Engineering, April 20-22, 1998, Eisenstadt (Austria).
Flach, Ph.; Hennes, M., 1998b. Die optische Turbulenz - wirklich nur ein limitierender Faktor für geodätische Messungen?. In: Freeden W. (ed.), Progress in Geodetic Science, Proceedings to Geodätische Woche Kaiserslautern (Germany), pp. 65-72.
Förstner, W., 1984. Quality Assessment of Object Location and Point Transfer using Digital Image Correlation Techniques. ISPRS, 25 (A3a), pp. 197-217.
Grün, A., 1985. Adaptive Least Square Correlation: A Powerful Image Matching Technique. South African Journal of Photogrammetry, Remote Sensing and Cartography, 14 (3), pp. 175-187.
Hennes, M., 1995. Entwicklung eines Messsystems zur Ermittlung von Turbulenzparametern der Atmosphäre für Anwendungen in der Geodäsie. Ph.D. Thesis, GIUB, DGK, Reihe C, Heft 438., pp. 76-102.
Hill, R., 1996. Algorithms for Obtaining Atmospheric Surface-Layer Fluxes from Scintillation Measurements. Journal of Atmospheric and Oceanic Technology, 14, pp. 456-467.
Hill, R. J; Clifford, S. F., 1978. Modified spectrum of atmospheric temperature fluctuations and its application to optical propagation. Journal of the Optical Society of America, 68 (7), pp. 892-899,.
Hufnagel, R. E., 1978. Propagation through Atmospheric Turbulence. In: Wolfe, W. L..; Zissis, G. J. (eds.), The Infrared Handbook, Office of Naval Research, Washington DC, Chapter 6, p. 9.
Huiser, A. M. J., Gächter, B. F., 1989. A solution to atmospherically induced problems in very high-accuracy alignment and levelling. Applied Physics, 22, pp. 1630-1638.
Kukkamäki, T. J., 1950. Über das Flimmern und Schweben des Zielbildes. Geofisica pura e applicata, 18, pp. 120-127.
Lawrence, R. S., Strohbehn, J. W., 1970. A Survey of Clear-Air Propagation Effects Relevant to Optical Communications. Proceedings of the IEEE, 58 (10), pp. 1523-1545.
Maas, H.-G., Stefanidis, A., Grün, A., 1994. From Pixels to Voxels - Tracking volume elements in sequences of 3D digital images. International Archives of Photogrammetry and Remote Sensing, 30, Part 3/2.
Papantoniou D., Dracos, T., 1989: Analyzing 3-D Turbulent Motions in Open Channel Flow by Use of Stereoscopy and Particle Tracking. In: Advances in Turbulence 2 (H.-H. Hernholz & H.E. Fiedler eds.), Springer Verlag, Heidelberg.
Tatarskii, V. I., 1971. The effects of the Turbulent Atmosphere on Wave Propagation. Keter Press, Jerusalem, pp. 166-215.
Thiermann, V., 1992. A displaced-beam scintillometer for line-averaged measurements of surface layer turbulence. Preprint Volume of the 10th Symposium on Turbulence and Diffusion, 29 Sept - 2 Oct. 1992, Portland, OR.
Vinogradov, V.V., Suchov, G. N., Medovikov, A.S., 1985. Opredelene refrakeji pri geodeziceskom nivelirovani po rozmytju regularnych struktur. UDK 528.024.4 / 535.3, Izv. vyss. ucebn. Zav. Geodezija Aerofotos"emka, 2 , Moskva, pp. 32-39.